

Nucleon Resonances in Kaon Photoproduction

C. BENNHOLD¹, T. MART^{1,2}, A. WALUYO¹, H. HABERZETTL¹, G. PENNER³,
T. FEUSTER³, U. MOSEL³

¹ Center for Nuclear Studies, Department of Physics, The George Washington University, Washington, D.C. 20052, U.S.A.

² Jurusan Fisika, FMIPA, Universitas Indonesia, Depok 16424, Indonesia

³ Institut für Theoretische Physik, Universität Giessen, D-35392 Giessen, Germany

Abstract. Nucleon resonances are investigated through the electromagnetic production of K-mesons. We study the kaon photoproduction process at tree-level and compare to a recently developed unitary K-matrix approach. Employing hadronic form factors along with the proper gauge prescription yields suppression of the Born terms and leads a resonance dominated process for both $K\Lambda$ and $K\Sigma$ photoproduction. Using new SAPHIR data we find the $K^+\Lambda$ photoproduction to be dominated by the $S_{11}(1650)$ at threshold, with additional contributions from the $P_{11}(1710)$ and $P_{13}(1720)$ states. The $K\Sigma$ channel couples to a cluster of Δ resonances around $W = 1900$ MeV. We briefly discuss some tantalizing evidence for a missing D_{13} resonance around 1900 MeV with a strong branching ratio into the $K\Lambda$ channel.

1 Introduction

Since its discovery five decades ago, the quark flavor strangeness has played a special role in nuclear physics and particle physics. More recently, the strange quark has found itself between two theoretical domains: on the one hand is the realm of chiral symmetry with the almost massless up and down quarks, while on the other side the physics can be described in terms of the heavy quark effective theory of the charm and bottom quarks. While the strange quark mass is too large to ensure convergence in SU(3) Chiral Perturbation Theory, it turns out to be too small to be safely included in heavy quark descriptions.

Among the successes of heavy quark physics is the straightforward description of excitation spectra of mesons and baryons that contain charm and bottom quarks. The excitation spectrum of nucleon and hyperon resonances, on the other hand, is still not well understood, despite 40 years of efforts in meson-baryon scattering and electromagnetic production processes. For this purpose, a number of laboratories like MAMI, ELSA, BATES, GRAAL and TJNAF have begun to address the issue of N^* physics, delivering new experimental data with unprecedented accuracy.

On the theoretical side, progress is being made in the understanding of N^* and Y^* properties from first principles calculations, such as lattice QCD which provides numerical solutions of QCD on a discrete space-time lattice. Due to the improved actions in the last few years, coupled with advances in algorithms and

computing power, the field is quickly moving towards providing new results in hadron phenomenology.

In order to provide a link between the new and improved data on one side and the results from lattice QCD on the other side, dynamical descriptions using hadronic degrees of freedom are required that can analyze the data in the various asymptotic reaction channels (like γN , πN , $\pi\pi N$, ηN , $K\Lambda$, $K\Sigma$ and others). In order to preserve unitarity and analyticity these analyses need to be performed in a unitary coupled-channels framework which allows separating background from resonance contributions. A number of different approaches have been developed over the last two decades [1, 2, 3, 4, 5], here we focus on the description of resonances within the effective Lagrangian framework.

2 The K -Matrix Born Approximation

Within the one-photon approximation, the full amplitude for any photoproduction process can be written in terms of a Bethe-Salpeter equation

$$M = V + V G T, \quad (1)$$

where V represents the driving term for the particular photoproduction process, G is the meson-baryon two-particle propagator, and T is the hadronic meson-baryon final state interaction. In principle, one would have to solve this equation as a four-dimensional integral equation. However in practice, due to the singularity structure involved, this has only recently been pursued for the case of pion scattering with a small number of diagrams in the driving term. Generally, a three-dimensional reduction is chosen that amounts to making an assumption of the intermediate two-particle propagator which then makes the calculations more tractable. Writing the full Bethe-Salpeter equation in the form

$$K = V + V \operatorname{Re}(G_{BS})K \quad (2)$$

$$T = K + iK \operatorname{Im}(G_{BS})T. \quad (3)$$

where G_{BS} is the full propagator, then any truncation of the first equation will still provide a unitary, albeit approximate, solution, as long as $i\operatorname{Im}(G_{BS})$ correctly describes the discontinuity across the scattering cut. Taking the special choice

$$\begin{aligned} iG_{BS} &= -2i(2\pi)^2 m_N \delta(k_N^2 - m_N^2) \delta(k_m^2 - m_m^2) \\ &\times \theta(k_N^0) \theta(k_m^0) (\not{k}_N + m_N), \end{aligned} \quad (4)$$

and $K = V$ leads to the simple K -matrix Born approximation:

$$T = \frac{V}{1 - iV}. \quad (5)$$

Thus, both intermediate particles are being placed on-shell. This procedure still allows for the resonance widths to be generated dynamically, while the

real part of the self-energy is absorbed in an effective resonance mass that is determined by the fit. The most recent coupled-channels approach that employs the K -matrix approximation within an effective Lagrangian framework has been performed by Feuster and Mosel [5]. They extract nucleon resonance parameters by simultaneously analyzing all available data for reactions involving the initial and final states $\gamma N, \pi N, \pi\pi N, \eta N$ and $K\Lambda$ up to $W = 1.9$ GeV.

3 Kaon Photoproduction in the Coupled-Channels Approach

While dynamical models involving various approximations for the Bethe-Salpeter equation are becoming increasingly successful in the description of pion photoproduction, the hadronic final state interaction in kaon photoproduction has usually been neglected. Without rescattering contributions the T -matrix is simply approximated by the driving term alone which is assumed to be given by a series of tree-level diagrams. Clearly, neglecting the final meson-baryon interaction in the full meson photoproduction T -matrix automatically leads to violation of unitarity since flux that can "leak out" into inelastic channels has not been properly accounted for. Enforcing unitarity dynamically requires solving a system of coupled channels with all possible final states. In principle, this would require information on channels, such as $K^+\Lambda \rightarrow K^+\Lambda$, for which no experimental information is available for obvious reasons. In practice, the coupling of the channels leads to an overdetermination of the free parameters, thus processes as the one mentioned above will be determined along with the experimentally accessible ones.

In contrast to eta photoproduction with the dominating $S_{11}(1535)$ resonance at low energies there is no single prominent resonance in the process $p(\gamma, K^+)\Lambda$ at low energies. The πN partial s - and p -waves do not show any cusp effect from the opening of the $K^+\Lambda$ threshold around $W = 1660$ MeV, in contrast to the very pronounced cusp at the ηN threshold visible in the S_{11} partial amplitude. The E_{0+} pion photoproduction multipole on the other hand, shown in Fig. 1, has some structure around the $K\Lambda$ threshold which may also be a signal of the $S_{11}(1650)$ state. This confluence of a resonance close to the $K^+\Lambda$ threshold certainly appears similar to the situation in the ηN channel. The real part of the M_{1-} multipole shows a small but clear signal around $W = 1600$ MeV, there is no known P_{11} resonance in this energy regime. As is obvious from Fig. 1, especially the imaginary parts of the multipoles are not well known at higher energies; new JLab data on pion photoproduction are expected to improve the situation.

The clearest indication of the coupling of the $K^+\Lambda$ channel to the πN channels appears to come in the inelastic cross sections, shown in Fig. 2. For the P_{11} channel the total $\pi N \rightarrow \pi\pi N$ cross section begins deviating from the total πN inelastic cross section at around $W = 1650$ MeV, clearly indicating the opening of another threshold.

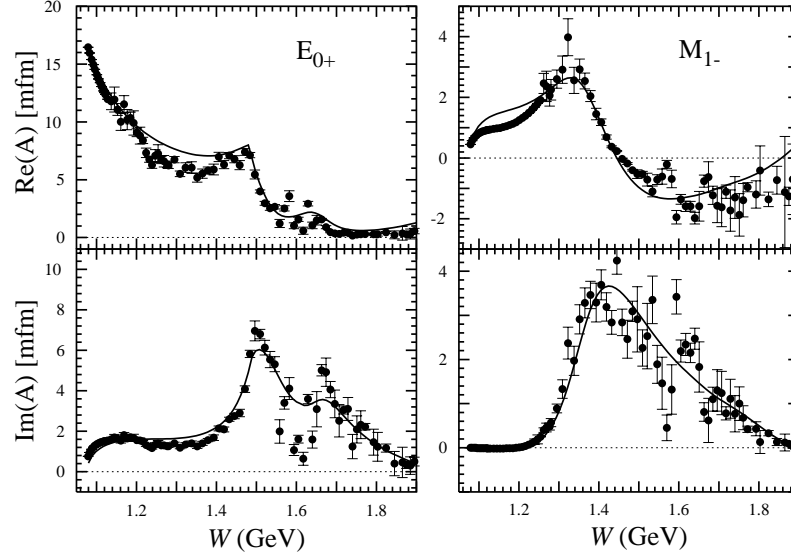


Fig. 1. Fits to the proton multipoles of pion photoproduction using the SP97 results of the VPI group. The solid curve shows the coupled-channels result of Ref. [5] in the K-matrix approximation.

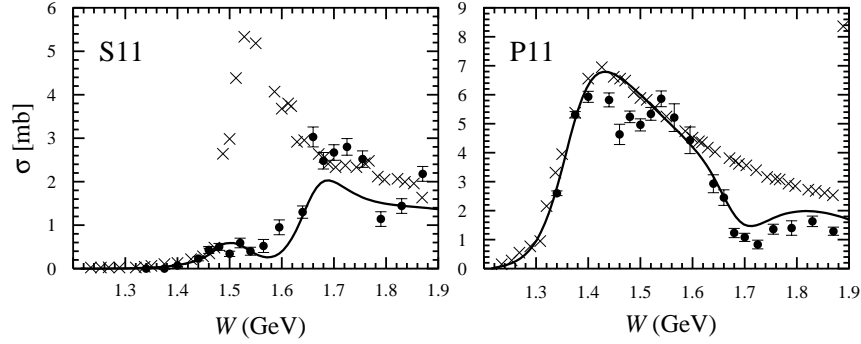


Fig. 2. Fits to the partial $\pi N \rightarrow \pi\pi N$ cross sections using the SM95 results of the VPI group. In addition, the total inelastic cross section (x) as determined from SM95 is shown. The notation is as in Fig.1.

Proper inclusion of rescattering effects into the kaon photoproduction process requires the accurate description of hadronic kaon production. Among the possible rescattering reactions, only $\pi N \rightarrow K\Lambda$ has been measured, processes such as $\eta N \rightarrow K\Lambda$ and $K\Lambda$ elastic scattering have to be determined through

the coupled channels approach. Figure 3 compares the coupled-channels result to available data. At threshold, only s - and p -waves contribute which receive their main contributions from the $S_{11}(1650)$ and $P_{11}(1710)$ resonances which are found to decay into the $K\Lambda$ channel with a branching ratio of about 6% and 14%, respectively. The strong forward peaking at higher energies is due mostly to the t -channel K^* contribution which contributes to all partial waves. Because of the magnitude of this contribution the t -channel vector meson contributions may need to be modified to reflect more closely a desired Regge-like behavior at high energies.

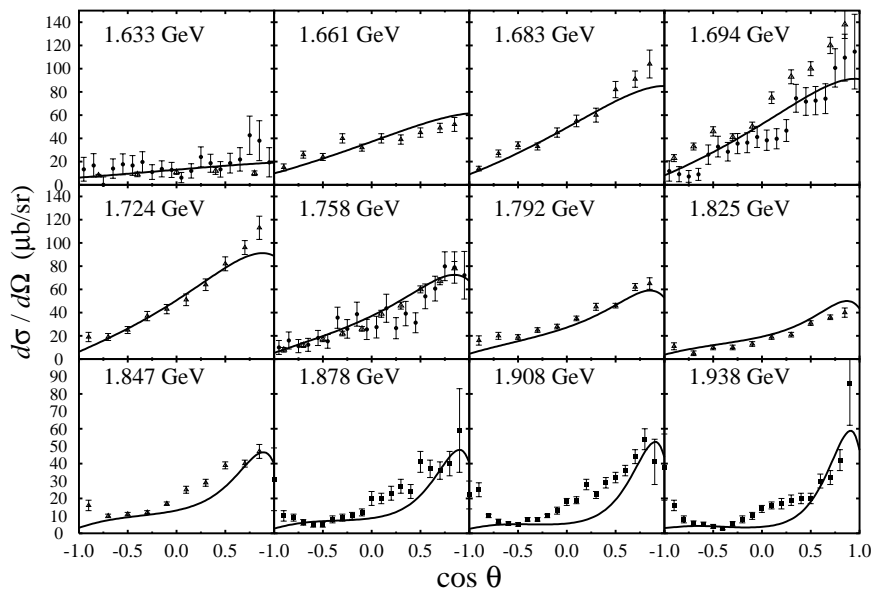


Fig. 3. The coupled-channels calculation of Ref. [5] compared to differential cross section data of the $\pi^-p \rightarrow K^0\Lambda$ reaction.

Including unitarity properly also raises the question of crossing symmetry which is straightforward to impose at the tree level [6, 7] but more involved in a coupled-channels framework. This becomes apparent when one compares the intermediate hadronic states of $p(\gamma, K^+)\Lambda$ with those of $p(K^-, \gamma)\Lambda$. While these two processes are related via crossing at the tree level, the photoproduction process proceeds through intermediate states with zero strangeness while the radiative capture reaction requires $S = -1$. At present, no Λ^* and Σ^* resonances have been included in our approach in order to limit the number of free parameters; thus crossing symmetry is violated.

4 Hadronic Form Factors and Gauge Invariance

It has been well known that including hadronic form factors at hadronic vertices in Fig. 4 can lead to the violation of gauge invariance in the Born amplitude. Furthermore, most isobaric models show a divergence at higher energies, which clearly demonstrates the need for a cut-off. Recent calculations [6, 8] demonstrated that many models which are able to describe (γ, K^+) experimental data tend to unrealistically overpredict the (γ, K^0) channel. The use of point-like particles disregards the composite nature of nucleons and mesons, thus losing the full complexity of a strongly interacting hadronic system

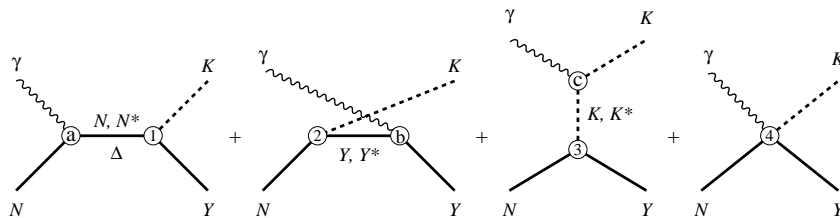


Fig. 4. Feynman diagrams for the electromagnetic production of kaons on the nucleon. Contributions from the Δ are only possible in Σ production. Electromagnetic vertices are denoted by (a), (b), and (c), hadronic vertices by (1), (2), and (3). The contact diagram (4) is required in both PS and PV couplings in order to restore gauge invariance after introducing hadronic form factors. The Born terms contain the N , Y , K intermediate states and the contact term.

In the model of Ref. [9] a hadronic form factor was introduced by multiplying the entire photoproduction amplitude [see Eq. (6) below] with an overall monopole form factor $F(\Lambda, t) = (\Lambda^2 - m_K^2)/(\Lambda^2 - t)$, where the cut-off mass Λ was treated as a free parameter. In spite of successfully minimizing the χ^2 while maintaining gauge invariance, there is no microscopic basis for this approach.

One method to handle the inclusion of such form factors has been proposed by Ohta [10]. By making use of minimal substitution Ohta has derived an additional amplitude which eliminates the form factors in the electric terms of the Born amplitude. Recently, Haberzettl [11, 12] has proposed another, more general method which allows for a multiplication of the electric terms with a form factor as well.

All amplitudes for photoproduction of pseudoscalar mesons have the general form

$$\mathcal{M}_{fi}(s, t, k^2) = \bar{u}(p_Y) \sum_{j=1}^4 A_j(s, t, k^2) M_j u(p_N), \quad (6)$$

where the M_j are Lorentz and gauge-invariant matrices and the functions A_j depend on kinematic variables, coupling constants and the resonance parameters.

The inclusion of form factors in the hadronic vertices of the Born terms in Fig. 4 leads to the modification of the four Born amplitudes A_j^{Born} . The amplitude for each resonance is separately gauge invariant, by construction. The amplitudes for kaon photoproduction are given by

$$A_1^{\text{Born}} = \frac{eg_{KYN}}{s - m_N^2} (Q_N + \kappa_N) F_1(\Lambda, s) + \frac{eg_{KYN}}{u - m_Y^2} (Q_Y + \kappa_Y) F_2(\Lambda, u) + \frac{eg_{KY'N}}{u - m_{Y'}^2} \kappa_T (1 - |Q_Y|) F_2(\Lambda, u), \quad (7)$$

$$A_2^{\text{Born}} = \frac{2eg_{KYN}}{t - m_K^2} \left(\frac{Q_N}{s - m_N^2} + \frac{Q_Y}{u - m_Y^2} \right) \tilde{F}, \quad (8)$$

$$A_3^{\text{Born}} = \frac{eg_{KYN}}{s - m_N^2} \frac{\kappa_N}{m_N} F_1(\Lambda, s), \quad (9)$$

$$A_4^{\text{Born}} = \frac{eg_{KYN}}{u - m_Y^2} \frac{\kappa_Y}{m_Y} F_2(\Lambda, u) + \frac{2eg_{KY'N}}{u - m_{Y'}^2} (1 - |Q_Y|) \frac{\kappa_T F_2(\Lambda, u)}{m_{Y'} + m_Y}, \quad (10)$$

where Q_N and Q_Y denote the charge of the nucleon and the hyperon in $+e$ unit, while κ_N , κ_Y , and κ_T indicate the anomalous magnetic moments of the nucleon, hyperon, and the transition of $\Sigma^0 \Lambda$. It is understood that $Y' = \Sigma^0$ [Λ] for $K\Lambda$ [$K\Sigma^0$] production. The difference between the three methods can be summarized as follows:

$$\tilde{F}_{\text{overall}} \text{ replaces } F_1, F_2, F_3, \text{ and } \tilde{F} \text{ [e.g., } \tilde{F}_{\text{overall}} = F_3(\Lambda, t)], \quad (11)$$

$$\tilde{F}_{\text{Ohta}} = 1, \quad (12)$$

$$\tilde{F}_{\text{Haberzettl}} = a_1 F_1(\Lambda, s) + a_2 F_2(\Lambda, u) + a_3 F_3(\Lambda, t), \quad (13)$$

with $a_1 + a_2 + a_3 = 1$.

Results of our previous calculations within the tree-level approximation that compare using an overall form factor with Ohta's method have previously been reported in Ref. [9, 13]. Here we compare the different methods with the one by Haberzettl [12] for kaon photoproduction, using a covariant vertex parameterization without any singularities on the real axis.

$$F_i(\Lambda, r_i) = \frac{\Lambda^2}{\sqrt{\Lambda^4 + (r_i - m_i^2)^2}}, \quad i = 1, 2, 3, \quad (14)$$

with $r_1 = s, r_2 = u, r_3 = t$ and $m_1 = m_N, m_2 = m_\Lambda, m_3 = m_K$.

Here we focus only on the magnitude of the leading Born coupling constants $g_{K\Lambda N}$ and $g_{K\Sigma N}$ extracted from the photoproduction data of $K^+\Lambda$ and $K^+\Sigma^0$. In contrast to the well-known πNN coupling constant, there are serious discrepancies between values for the KYN coupling constants extracted from

Table 1.

The leading coupling constants g_{KAN} and $g_{K\Sigma N}$, the hadronic form factor cut-off Λ , and the χ^2/N from fitting to kaon photoproduction data using different methods of restoring gauge invariance within the tree-level approximation.

form factor coupling		$g_{KAN}/\sqrt{4\pi}$	$g_{K\Sigma N}/\sqrt{4\pi}$	Λ (GeV)	χ^2/N
method	constants				
no	fixed	-3.80	1.20	-	55.76
no	free	-1.90	-0.37	-	3.33
overall	fixed	-3.80	1.20	0.213	2.84
Ohta	fixed	-3.80	1.20	1.422	14.21
Haberzettl	fixed	-3.80	1.20	1.128	4.63
SU(3)	-	-3.70 ± 0.70	1.10 ± 0.20	-	-

electromagnetic reactions and those from hadronic processes which tend to be closer to accepted SU(3) values.

Our numerical results for the coupling constants using the different methods are summarized in Table 1, in comparison to the predictions of SU(3). If the leading coupling constants $g_{KAN}/\sqrt{4\pi}$ and $g_{K\Sigma N}/\sqrt{4\pi}$ are not allowed to vary freely and are fixed at reasonable SU(3) values of -3.80 and 1.20 (close to what is obtained from hadronic reactions [14]), the χ^2 obtained in our model *without* hadronic form factors comes out to be 55.8 . On the other hand, if the two couplings are allowed to vary freely, one obtains $g_{KAN}/\sqrt{4\pi} = -1.90$ and $g_{K\Sigma N}/\sqrt{4\pi} = -0.37$ with $\chi^2/N = 3.3$. In spite of the small χ^2/N in the latter case, this result obviously indicates that either there is a very large amount of SU(3) symmetry breaking or that important physics has been left out in the extraction of coupling constants from the (γ, K) processes. In Ref. [12], we advocate the second position and demonstrate that the inclusion of structure at the hadronic vertex permits an adequate description of kaon photoproduction with couplings close to the SU(3) values, provided one uses the appropriate gauge procedure.

Figure 5 compares the different gauge prescriptions to the new kaon photoproduction data from SAPHIR [15]. Especially at threshold and at higher energies, it is evident that the method of Ref. [12] is superior to the approach by Ohta.

5 Kaon Photoproduction in the Tree-Level Approximation

Almost all previous analyses of kaon photoproduction were performed at tree level [6, 7, 8, 9]. While this leads to the violation of unitarity as discussed above,

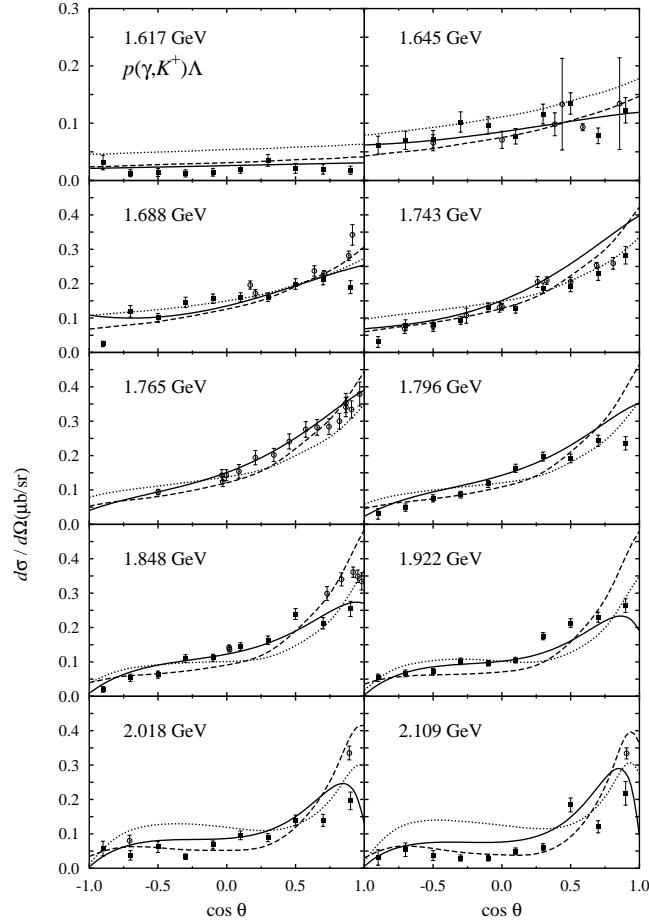


Fig. 5. Differential cross section for the $p(\gamma, K^+)\Lambda$ channel. In the K-matrix approximation the dotted curves have been obtained with Ohta's prescription, the dashed curves are due to Haberzettl's method. The solid curves show a tree-level calculation (Set II of Table 2) with Haberzettl's method. Old data are shown by open circles, new SAPHIR data by solid squares [15].

this kind of isobaric model provides a simple tool to parameterize meson photoproduction off the nucleon because it is relatively easy to calculate and to use for production on nuclei. Without rescattering contributions the T -matrix is simply approximated by the driving term alone which is assumed to be given by a series of tree-level diagrams. The selected Feynman diagrams for the s -, u -, and t -channel contain some unknown coupling parameters to be adjusted

in order to reproduce experimental data. Final state interaction is effectively absorbed in these coupling constants which then cannot easily be compared to couplings from other reactions. Guided by the coupled-channel results we have therefore constructed a tree-level amplitude that reproduces all available $K^+\Lambda$, $K^+\Sigma^0$ and $K^0\Sigma^+$ data and thus provides an effective parameterization of the process. In this model, we include the three resonances that have been found in the coupled-channels approach to decay into the $K\Lambda$ channel, the $S_{11}(1650)$, $P_{11}(1710)$, and $P_{13}(1720)$. For $K\Sigma$ production we also allow contributions from the $S_{31}(1900)$ and $P_{31}(1910)$ Δ resonances. Furthermore, we include not only the usual 1^- vector meson $K^*(892)$, but also the 1^+ pseudovector meson $K_1(1270)$ in the t -channel since a number of studies [6, 7, 16] have found this resonance to give a significant contribution.

In order to describe all six isospin channels of $K\Lambda$ and $K\Sigma$ simultaneously we invoke isospin symmetry for the strong coupling constants

$$g_{K^+\Lambda p} = g_{K^0\Lambda n} , \quad (15)$$

$$g_{K^+\Sigma^0 p} = -g_{K^0\Sigma^0 n} = g_{K^0\Sigma^+ p}/\sqrt{2} = g_{K^+\Sigma^- n}/\sqrt{2} , \quad (16)$$

$$g_{K^+\Sigma^0 \Delta^+} = g_{K^0\Sigma^0 \Delta^0} = -\sqrt{2}g_{K^0\Sigma^+ \Delta^+} = \sqrt{2}g_{K^+\Sigma^- \Delta^0} . \quad (17)$$

The electromagnetic resonance couplings of the proton and the neutron are related to helicity amplitudes. For spin 1/2 resonances we have

$$\frac{g_{N^{*0}n\gamma}}{g_{N^{*+}p\gamma}} = \frac{A_{1/2}^n}{A_{1/2}^p} , \quad (18)$$

while there are two couplings for spin-3/2 resonances

$$\frac{g_{N^{*0}n\gamma}^{(1)}}{g_{N^{*+}p\gamma}^{(1)}} = \frac{\sqrt{3}A_{1/2}^n \pm A_{3/2}^n}{\sqrt{3}A_{1/2}^p \pm A_{3/2}^p} , \quad (19)$$

$$\frac{g_{N^{*0}n\gamma}^{(2)}}{g_{N^{*+}p\gamma}^{(2)}} = \frac{\sqrt{3}A_{1/2}^n - (m_N/m_{N^*})A_{3/2}^n}{\sqrt{3}A_{1/2}^p - (m_N/m_{N^*})A_{3/2}^p} \quad (20)$$

The helicity amplitudes quoted in the Particle Data Tables [17] have large error bars, especially for the neutron values. We use the following values for the ratios: $g_{S_{11}(1650)n\gamma}/g_{S_{11}(1650)p\gamma} = -0.28$, $g_{P_{11}(1710)n\gamma}/g_{P_{11}(1710)p\gamma} = -0.22$, and $g_{P_{13}(1720)n\gamma}^{(1)}/g_{P_{13}(1720)p\gamma}^{(1)} = -2.24$, $g_{P_{13}(1720)n\gamma}^{(2)}/g_{P_{13}(1720)p\gamma}^{(2)} = 0.42$ for the various resonances.

For neutral kaon photoproduction the transition moments $g_{K^{*+}K^+\gamma}$ in K^+ photoproduction must be replaced by the neutral transition moment $g_{K^{*0}K^0\gamma}$. The transition moment is related to the decay width which are well known for the $K^*(892)$, i.e.

$$\Gamma_{K^{*+} \rightarrow K^+\gamma} = 50 \pm 5 \text{ keV} , \quad (21)$$

$$\Gamma_{K^{*0} \rightarrow K^0\gamma} = 117 \pm 10 \text{ keV} . \quad (22)$$

Thus, we obtain $g_{K^{*0}K^0\gamma} = -1.53 g_{K^{*+}K^+\gamma}$, where we have used a quark model prediction to constrain the relative sign.

The decay widths of $K_1(1270)$, on the other hand, are not well known. We therefore take the ratio of the charged to neutral moment of the $K_1(1270)$ as a free parameter that is fixed by data in the $p(\gamma, K^0)\Sigma^+$ channel.

In order to approximately account for unitarity corrections at tree-level we include energy-dependent widths in the resonance propagators

$$\Gamma(\mathbf{q}) = \Gamma_{N^*} \frac{\sqrt{s}}{m_{N^*}} \sum_i x_i \left(\frac{|\mathbf{q}_i|}{|\mathbf{q}_i^{N^*}|} \right)^{2l+1} \frac{D_l(|\mathbf{q}_i|)}{D_l(|\mathbf{q}_i^{N^*}|)} , \quad (23)$$

where the sum runs over the possible decay channels into a meson and a baryon with mass m_i and m_b , respectively, and relative orbital angular momentum l . In Eq. (23), Γ_{N^*} represents the total decay width and x_i denotes the relative branching ratio of the resonance into the i th channel. The final state momenta are given by $|\mathbf{q}_i^{N^*}| = [(m_{N^*}^2 - m_b^2 + m_i^2)^2 / 4m_{N^*}^2 - m_i^2]^{1/2}$, and $|\mathbf{q}_i| = [(s - m_b^2 + m_i^2)^2 / 4s - m_i^2]^{1/2}$, while the fission barrier factor $D_l(\mathbf{q})$ is chosen as $D_l(\mathbf{q}) = \exp(-\mathbf{q}^2/3\alpha^2)$ with $\alpha = 410 \text{ MeV}$.

We have performed a combined fit to all differential cross section and recoil polarization data of $p(\gamma, K^+)A$ and $p(\gamma, K^+)\Sigma^0$. The $p(\gamma, K^0)\Sigma^+$ channel is included later, since data for this channel have large error bars, and therefore do not strongly influence the fit. The results of our fits are summarized in Table 2. We compare our present study to an older model [9] which employed an overall hadronic form factor and did not contain the $P_{13}(1720)$ and the $K_1(1270)$ states. The significant improvement in χ^2 comes mostly from including the $P_{13}(1720)$ in the KA channel; its decay into the $K\Sigma$ channel is negligible. A further reduction in χ^2 results from allowing the non-resonant background terms to have a different form factor cut-off than the s -channel resonances. For the former, the fit produced a soft value of about 800 MeV, leading to a strong suppression of the background terms while the resonance cut-off is determined to be 1.89 GeV. This combination leads to a reaction mechanism which is resonance dominated in all isospin channels. Table 2 reveals that the coupling ratio $K_1^0 K^0\gamma / K_1^+ K^+\gamma$ is obtained with large uncertainty. This comes as no surprise since the data in the $p(\gamma, K^0)\Sigma^+$ channel have large error-bars; we predict the ratio of the decay widths to be

$$\frac{\Gamma_{K_1^0 \rightarrow K^0\gamma}}{\Gamma_{K_1^+ \rightarrow K^+\gamma}} = 0.068 \pm 0.110 . \quad (24)$$

Table 2.

Coupling constants fitted in our model. Set I results from using our previous model which fits old photo- and electroproduction data [9], set II shows the result of this study. Note that we have used the following parameterization of the form factor of Eq. (14): $\tilde{F} = \sin^2 \Theta_{\text{hd}} \cos^2 \Phi_{\text{hd}} F(\Lambda, s) + \sin^2 \Theta_{\text{hd}} \sin^2 \Phi_{\text{hd}} F(\Lambda, u) + \cos^2 \Theta_{\text{hd}} F(\Lambda, t)$, where the combination of sinusoidal functions ensures the correct normalization of the form factor. Both Θ_{hd} and Φ_{hd} are obtained from the fit. Λ_1 refers to the cut-off for the background terms while Λ_2 denotes the resonance cut-off.

Coupling constants	Set I	Set II
$g_{KAN}/\sqrt{4\pi}$	-3.094 ± 0.077	-3.800
$g_{K\Sigma N}/\sqrt{4\pi}$	1.227 ± 0.055	1.200
$\Theta_{\text{hd}} (^{\circ})$	-	108 ± 4
$\Phi_{\text{hd}} (^{\circ})$	-	90 ± 6
Λ_1 (GeV)	0.853 ± 0.018	0.798 ± 0.006
Λ_2 (GeV)	-	1.883 ± 0.110
<i>K</i> Λ coupling		
$g_{K^*K\gamma} g_{K^*\Lambda N}^V/4\pi$	-0.188 ± 0.006	-0.506 ± 0.013
$g_{K^*K\gamma} g_{K^*\Lambda N}^T/4\pi$	-0.122 ± 0.018	0.672 ± 0.065
$g_{K_1K\gamma} g_{K_1\Lambda N}^V/4\pi$	-	0.063 ± 0.073
$g_{K_1K\gamma} g_{K_1\Lambda N}^T/4\pi$	-	0.372 ± 0.209
$g_{N^*(1650)N\gamma} g_{KAN^*(1650)}/\sqrt{4\pi}$	-0.063 ± 0.005	-0.130 ± 0.001
$g_{N^*(1710)N\gamma} g_{KAN^*(1710)}/\sqrt{4\pi}$	-0.065 ± 0.019	-0.094 ± 0.011
$g_{N^*(1720)N\gamma}^{(1)} g_{KAN^*(1720)}/\sqrt{4\pi}$	-	0.060 ± 0.003
$g_{N^*(1720)N\gamma}^{(2)} g_{KAN^*(1720)}/\sqrt{4\pi}$	-	0.943 ± 0.021
<i>K</i> Σ coupling		
$g_{K^*K\gamma} g_{K^*\Sigma N}^V/4\pi$	-0.079 ± 0.005	-0.306 ± 0.013
$g_{K^*K\gamma} g_{K^*\Sigma N}^T/4\pi$	-0.079 ± 0.020	-0.603 ± 0.017
$g_{K_1K\gamma} g_{K_1\Sigma N}^V/4\pi$	-	-0.397 ± 0.038
$g_{K_1K\gamma} g_{K_1\Sigma N}^T/4\pi$	-	-1.710 ± 0.216
$g_{N^*(1650)N\gamma} g_{K\Sigma N^*(1650)}/\sqrt{4\pi}$	-0.007 ± 0.015	-0.041 ± 0.003
$g_{N^*(1710)N\gamma} g_{K\Sigma N^*(1710)}/\sqrt{4\pi}$	2.100 ± 0.102	0.084 ± 0.018
$g_{\Delta(1900)N\gamma} g_{K\Sigma\Delta(1900)}/\sqrt{4\pi}$	0.234 ± 0.015	0.104 ± 0.002
$g_{\Delta(1910)N\gamma} g_{K\Sigma\Delta(1910)}/\sqrt{4\pi}$	-0.991 ± 0.091	0.363 ± 0.017
$g_{K_1^0 K^0 \gamma} / g_{K_1^+ K^+ \gamma}$	-	0.261 ± 0.210
χ^2/N	5.99	3.45

The differential cross section of $p(\gamma, K^+)A$ was already shown in Fig. 5, where we compare the tree-level fit (Set II in Table 2) with coupled-channel results. At threshold, the process is dominated by s -wave, coming from the $S_{11}(1650)$ state. At higher energies we find strong forward peaking similar to the $p(\pi^-, K^0)A$ case that can again be attributed to the K^* contribution.

The comparison of the two models with the $p(\gamma, K^+)\Sigma^0$ data is shown in Fig. 6 from threshold up to 2.2 GeV. In contrast to K^+A photoproduction, this channel contains significant p - and d -wave contributions already at threshold. This points to the $P_{11}(1710)$ state as an important resonance in low-energy $K\Sigma$ production; here the $S_{11}(1650)$ lies below threshold. This finding is consistent with a recent study [18] of $K\Sigma$ production in NN scattering, $NN \rightarrow NK\Sigma$, where the $P_{11}(1710)$ state was identified as a major contribution.

Figure 7 compares the two models for the $p(\gamma, K^0)\Sigma^+$ channel. The new SAPHIR data are clearly able to discriminate between the models. The model corresponding to Set I not only overpredicts the data at threshold, but also yields a backward peaking behavior, while the data tend to favour forward peaking. This dramatically different behavior is due mostly to the different gauge prescriptions used since this influences the relative contribution of the background terms. As mentioned above, Set I used an overall hadronic form factor that multiplied the entire amplitude, while Set II employs the mechanism by Haberzettl, which is clearly preferred by the data.

Figure 8 compares total cross section data for the three different K^+ photoproduction reactions on the proton. For $p(\gamma, K^+)A$ one can clearly see the cusp effect around $W = 1710$ MeV, indicating the opening of the $K\Sigma$ channel. The steep rise of the K^+A data at threshold is again indicative of a strong s -wave. The $K^+\Sigma^0$ data rise more slowly at threshold, suggesting p - and d -wave, rather than s -wave, dominance. Furthermore, there is a clear evidence for a resonance structure around $W = 1900$ MeV. There is indeed a cluster of six or seven Δ resonances with spin quantum numbers $1/2, 3/2, 5/2$ and $7/2$; it is at this energy that the total $K\Sigma$ cross section reaches its maximum. Coupled-channels calculations for the $K\Sigma$ reaction are in progress and will be reported elsewhere.

The recoil polarization for K^+A and $K^+\Sigma^0$ production is shown in Fig. 9 and Fig. 10, respectively. We find good agreement with the data using Set II of Table 2, while the older model (Set I) gives almost zero polarization throughout this energy range. The main reason for this dramatic difference is the more prominent role that the resonances play in the present model, defined by Set II. However, this model utterly fails to reproduce the polarization data for $K^+\Sigma^0$ production. Since the recoil polarization observable is sensitive especially to the imaginary parts of the amplitudes this discrepancy suggests that we do not have the correct resonance input for the $K\Sigma$ channel.

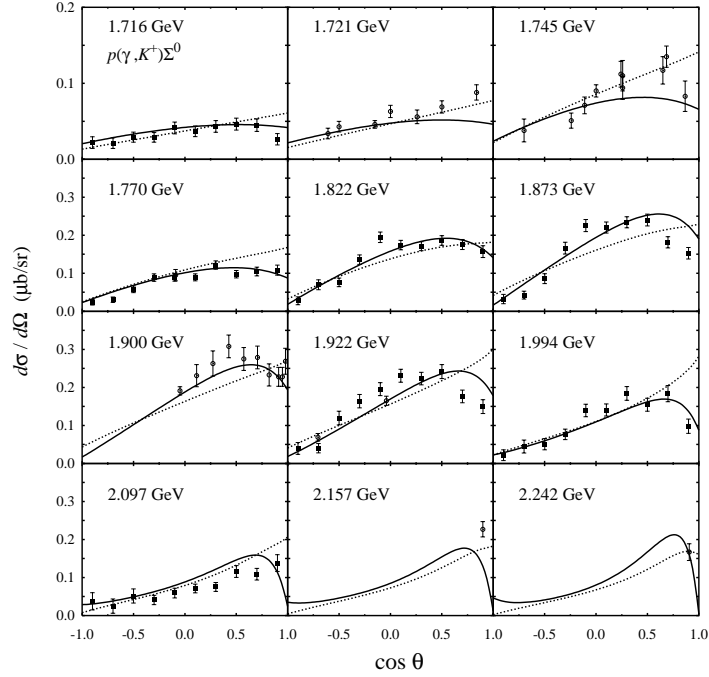


Fig. 6. Differential cross section for $p(\gamma, K^+)\Sigma^0$ channel calculated at tree level. The solid curve shows Set II of Table 2 while the dashed line shows the older model, Set I of Table 2.

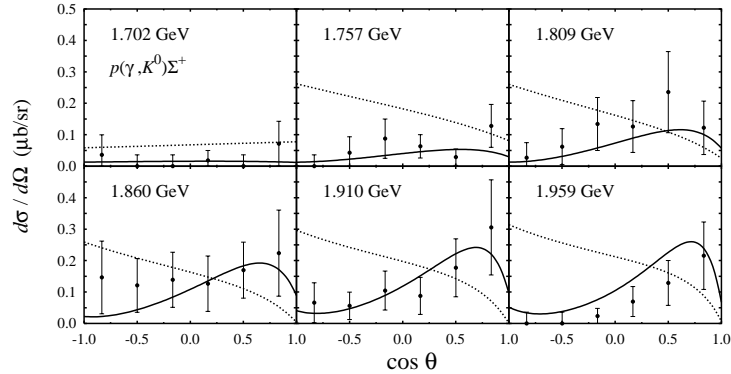


Fig. 7. Differential cross section for $p(\gamma, K^0)\Sigma^+$ channel. Data are from Ref. [13]. Notation is as in Fig. 6.

6 Kaon Photoproduction: a Signal for "Missing" Resonances?

A recent quark model study of Capstick and Roberts [19] finds that a number of missing and undiscovered nucleon resonances have substantial decay ampli-

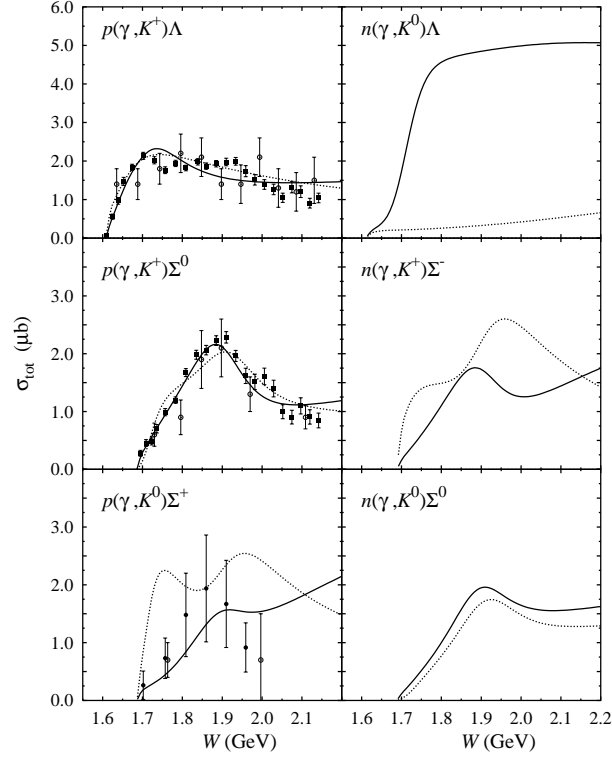


Fig. 8. Total cross sections for the six isospin channels of kaon photoproduction on the nucleon. The data for K^+ production come from Ref. [15] and the data for K^0 production are from Ref. [13]. The notation of the curves is as in Fig. 6.

tudes into the $K\Lambda$ and $K\Sigma$ final states. They conclude that electromagnetic and hadronic kaon production in the energy region of 1.8 - 2.3 GeV can provide a useful tool to identify new states and help to extract resonance parameters of weakly established states. Most of these resonances appear to be negative-parity states with wave functions predominantly in the $N = 3$ band.

The new SAPHIR total cross section data in the $K^+\Lambda$ channel (shown in Fig. 8) reveal an interesting structure around $W = 1900$ MeV. Our model fits currently do not reproduce this bump since there is no well-established (3- and 4-star) $I=1/2$ state at this energy. However, Ref. [19] predicts a missing D_{13} at 1960 MeV that has a large branching ratio into the $K\Lambda$ channel. In order to study this structure more closely, we have included a D_{13} resonance into our Set II model but have allowed the mass and the width of the state to vary as free parameters. We achieve a significant reduction in χ^2/N for a mass of 1902

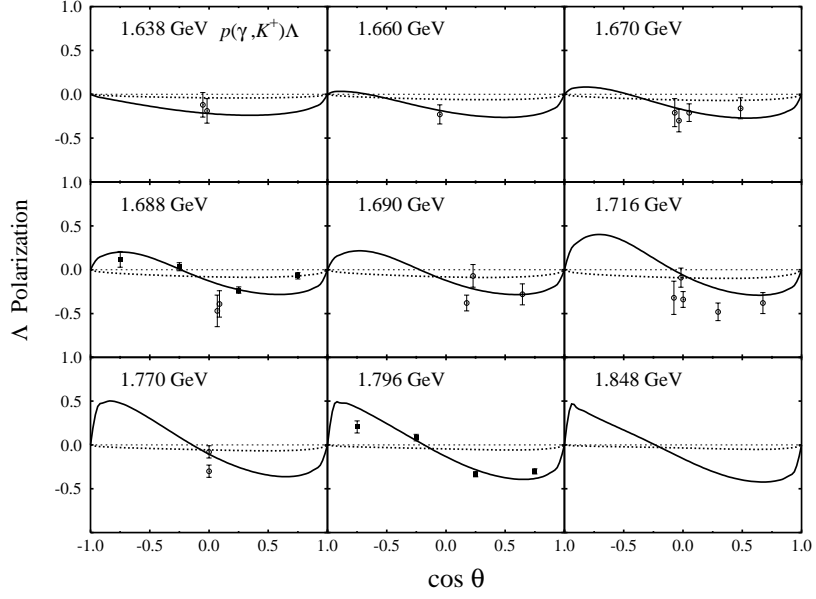


Fig. 9. Λ recoil polarization for $p(\gamma, K^+)\Lambda$. Notation is as in Fig. 6.

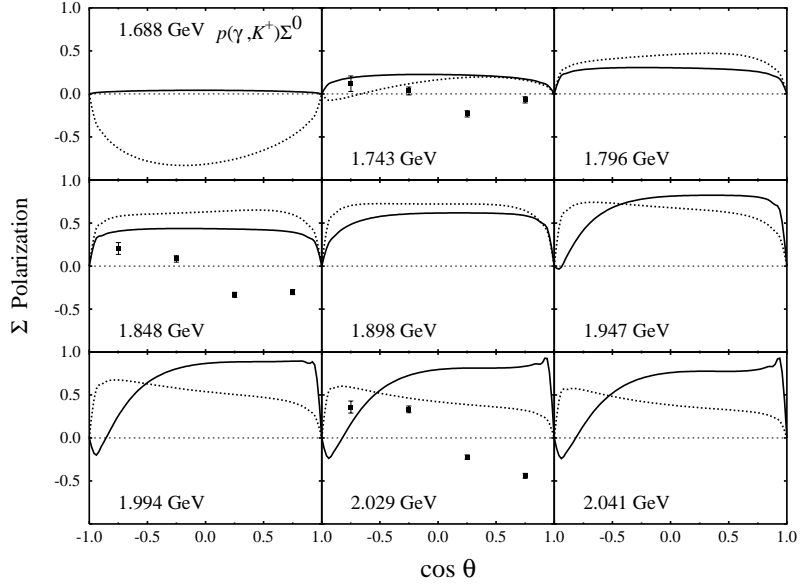


Fig. 10. Σ^0 recoil polarization of $p(\gamma, K^+)\Sigma^0$. Notation is as in Fig. 6.

MeV and a total width of 315 MeV. While this clearly cannot yet be regarded as proof for the existence of this state it nevertheless demonstrates the potential of kaon production as a tool to discover missing nucleon resonances.

This work was supported by DOE grant DE-FG02-95ER-40907 (CB,AW, and HH), a University Research for Graduate Education (URGE) grant (TM), BMBF, DFG and GSI Darmstadt (GP, TF, and UM).

References

1. R.E. Cutkosky *et al.*, Phys. Rev. D **20**, 2839 (1979).
2. G. Hoehler *et al.* *Handbook of Pion-Nucleon Scattering*, Physics Data No. 12-1 (1979).
3. D.M. Manley and E.M. Saleski, Phys. Rev. D **45**, 4002 (1992).
4. R.A. Arndt *et al.* Phys. Rev. C **52**, 2120 (1995).
5. T. Feuster and U. Mosel, Phys. Rev. C **58**, 457 (1998); *Photon and Meson Scattering on the Nucleon*, nucl-th/9803057, Phys. Rev. C (in press).
6. J. C. David *et al.* Phys. Rev. C **53**, 2613 (1996).
7. R. A. Williams *et al.* Phys. Rev. C **46**, 1617 (1992).
8. T. Mart *et al.* Phys. Rev. C **51**, R1074 (1995).
9. C. Bennhold, T. Mart, and D. Kusno, *Proceedings of the CEBAF/INT Workshop on N^* Physics*, Seattle, USA, 1996 (World Scientific, Singapore, 1997, T.-S. H. Lee and W. Roberts, editors), p.166.
10. K. Ohta, Phys. Rev. C **40**, 1335 (1989).
11. H. Haberzettl, Phys. Rev. C **56**, 2041 (1997).
12. H. Haberzettl *et al.* Phys. Rev. C **58**, R40 (1998).
13. C. Bennhold *et al.* Nucl. Phys. A **639**, 209c (1998).
14. R. G. E. Timmermans *et al.* Nucl. Phys. A **585**, 143c (1995).
15. Saphir Collaboration (M.Q. Tran *et al.*) "Measurement of $\gamma p \rightarrow K^+ \Lambda$ and $K^+ \Sigma^0$ at photon energy up to 2 GeV", accepted for publication in Phys. Lett. B.
16. R. A. Adelseck and L. E. Wright, Phys. Rev. C **38**, 1965 (1988).
17. Particle Data Group, Eur. Phys. J. C **3**, 1 (1998).
18. A. Sibirtsev *et al.*, nucl-th/9810070.
19. S. Capstick and W. Roberts, *nucl-th/9804070*.